Journal of Experimental Botany, Vol. 75, No. 8 pp. 2299–2312, 2024
https://doi.org/10.1093/jxb/erae035 Advance Access Publication 1 February 2024

RESEARCH PAPER

Contrasting cytosolic glutathione redox dynamics under abiotic and biotic stress in barley as revealed by the biosensor Grx1–roGFP2

Finja Bohle[1,2], Alina Klaus[3], Julian Ingelfinger[1], Hendrik Tegethof[2,†], Nassim Safari[4], Markus Schwarzländer[5], Frank Hochholdinger[3], Matthias Hahn[4], Andreas J. Meyer[2], Ivan F. Acosta[6], and Stefanie J. Müller-Schüssele[1,*]

[1] Molecular Botany, Department of Biology, RPTU Kaiserslautern-Landau, D-67633 Kaiserslautern, Germany
[2] Chemical Signalling, Institute of Crop Science and Resource Conservation (INRES), University of Bonn, D-53113 Bonn, Germany
[3] Crop Functional Genomics, Institute of Crop Science and Resource Conservation (INRES), University of Bonn, D-53113 Bonn, Germany
[4] Phytopathology, Department of Biology, RPTU Kaiserslautern-Landau, D-67633 Kaiserslautern, Germany
[5] Institute of Plant Biology and Biotechnology, University of Münster, D-48143 Münster, Germany
[6] Max Planck Institute for Plant Breeding Research, D-50829 Cologne, Germany
[†] Present address: Miltenyi Biotec B.V. & Co. KG, D-51429 Bergisch Gladbach, Germany.

* Correspondence: mueschue@rptu.de

Received 11 January 2024; Editorial decision 23 January 2024; Accepted 29 January 2024

Editor: Saijaliisa Kangasjärvi, University of Helsinki, Finland

Abstract

Barley is a staple crop of major global importance and relatively resilient to a wide range of stress factors in the field. Transgenic reporter lines to investigate physiological parameters during stress treatments remain scarce. We generated and characterized transgenic homozygous barley lines (cv. Golden Promise Fast) expressing the genetically encoded biosensor Grx1–roGFP2, which indicates the redox potential of the major antioxidant glutathione in the cytosol. Our results demonstrated functionality of the sensor in living barley plants. We determined the glutathione redox potential (E_{GSH}) of the cytosol to be in the range of –308 mV to –320 mV. E_{GSH} was robust against a combined NaCl (150 mM) and water deficit treatment (–0.8 MPa) but responded with oxidation to infiltration with the phytotoxic secretome of the necrotrophic fungus *Botrytis cinerea*. The generated reporter lines are a novel resource to study biotic and abiotic stress resilience in barley, pinpointing that even severe abiotic stress leading to a growth delay does not automatically induce cytosolic E_{GSH} oxidation, while necrotrophic pathogens can undermine this robustness.

Keywords: Crop, genetically encoded biosensor, glutathione redox potential, *Hordeum vulgare*, redox-sensitive GFP, water deficit.

Introduction

Barley (*Hordeum vulgare*) is among the most important crop species worldwide (Newton *et al.*, 2011) and exhibits a high abiotic stress tolerance as compared with other cereal crops (FAO, https://www.fao.org/3/Y4263E/y4263e0e.htm; Munns *et al.*, 2006). Varieties, landraces, and wild barley accessions constitute a valuable genetic reservoir for crop improvement in the face of progressing climate change (Dawson *et al.*, 2015; Muzammil *et al.*, 2018). Several markers affecting winter survival, flowering time, and abiotic stress tolerance have already been identified and are used in breeding (Newton *et al.*, 2011; Dawson *et al.*, 2015; Muzammil *et al.*, 2018). Transcriptomic datasets investigating the response of barley to salt and/or water deficit identified oxidation–reduction processes as part of the stress response, especially after several days of stress exposure (Kreszies *et al.*, 2019; Osthoff *et al.*, 2019). Biotic stresses, in particular fungal diseases such as rust, powdery mildew, *Fusarium* head blight, and *Rhizoctonia* root rot, can affect barley in a similar manner to wheat or other cereal grasses.

With its diploid, sequenced genome (Mascher *et al.*, 2017), barley is a prime genetic model for the cereal grasses of the *Triticeae* tribe. Moreover, the variety Golden Promise is genetically accessible via embryo transformation (Imani *et al.*, 2011; Amanda *et al.*, 2022). Drought stress affects plant height, developmental timing, and spikelet development with a role for *PHOTOPERIOD-H1* (*Ppd-H1*), as demonstrated via introgression lines (Gol *et al.*, 2021). However, while transgenic reporter lines are a standard research tool in other model plants, only a few fluorescent reporter lines have been generated to gain insight into barley growth and physiology, such as, for example, auxin and cytokinin signalling (Kirschner *et al.*, 2018; Amanda *et al.*, 2022) or calcium signatures (Giridhar *et al.*, 2022).

Genetically encoded biosensors are fluorescent proteins (or protein pairs) that change their properties specifically in response to a physiological parameter. Like any other protein, they can be targeted to specific subcellular localizations with targeting signals. The development and characterization of biosensors for a wide array of physiological parameters has paved the way for the specific assessment of physiological states of subcellular compartments, ultimately challenging and shifting many paradigms of cell biology (reviewed in Meyer *et al.*, 2021; Müller-Schüssele *et al.*, 2021b). For example, the redox potential of the redox pair of reduced glutathione (GSH) and its oxidized form glutathione disulfide (GSSG) has been revealed to be far from its midpoint potential in subcellular compartments harbouring a glutathione reductase (GR), with only nanomolar amounts of GSSG present. This results in glutathione redox potentials (E_{GSH}) as low as approximately −320 mV in the cytosol of plant cells, making the largely reduced pool of glutathione a versatile electron donor reservoir for enzymes that draw electrons from GSH to perform reduction reactions. This includes enzymes involved in the scavenging of reactive oxygen species (ROS) or oxidative damage repair, such as dehydroascorbate reductase (DHAR) or atypical methionine sulfoxide reductases B (MSRB1) (Foyer and Noctor, 2011; Rey and Tarrago, 2018; Müller-Schüssele *et al.*, 2021a). The compartment-specific study of E_{GSH} has been largely driven by the characterization of redox-sensitive green fluorescent protein 2 (roGFP2) (Meyer *et al.*, 2007; Schwarzländer *et al.*, 2008) that contains a GSH-dependent thiol switch on the outer face of the GFP β-barrel structure. The redox status of this cysteine pair is dependent on E_{GSH}, while reaction kinetics are accelerated by class I glutaredoxin (GRX) catalysis, resulting in roGFP2 linked to human glutaredoxin 1 (Grx1–roGFP2) as the most widely used E_{GSH} biosensor (Gutscher *et al.*, 2008; Schwarzländer *et al.*, 2016; Müller-Schüssele *et al.*, 2021b).

The study of redox networks in *Arabidopsis thaliana* has already revealed that glutathione-dependent and thioredoxin-dependent systems can at least partially compensate for each other in mitochondria and the cytosol (Marty *et al.*, 2009, 2019). This partially redundant input of electrons via GR or thioredoxin reductase A and B (NTRA and NTRB), both of which are NADPH dependent, largely prohibits oxidation of the glutathione pool. Nevertheless, null mutants of the cytosolic/peroxisomal glutathione reductase 1 (*gr1-1* and *gr1-2*) show a less negative cytosolic E_{GSH} than the wild type (WT) (Marty *et al.*, 2009) with enhanced oxidation after osmotic stress (300 mM mannitol) (Bangash *et al.*, 2019). In WT *A. thaliana*, oxidative shifts in cytosolic E_{GSH} have been observed under oxygen deprivation (Wagner *et al.*, 2019), heat or heavy metal stress (Schwarzländer *et al.*, 2009), and after herbicide treatment of chloroplasts (Ugalde *et al.*, 2021). Cyst nematode parasitism induced a slight oxidative shift in cytosolic E_{GSH} measured via Grx1–roGFP2 in *A. thaliana* (Hasan *et al.*, 2022). Interestingly, glutathione was required for wound-induced resistance of *A. thaliana* to *Botrytis cinerea* (Chassot *et al.*, 2008). Most studies targeting biotic stresses have focused on the response to defence elicitors, also referred to as pathogen-associated molecular patterns (PAMPs). Treatment of leaf tissue with bacterial or fungal PAMPs induces a transient extracellular oxidative burst, which was monitored from an intracellular perspective using Grx1–roGFP2 or roGFP2–Orp1 (Nietzel *et al.*, 2019; Ugalde *et al.*, 2022; Arnaud *et al.*, 2023). To date, no data are available about the impact of infection by necrotrophic fungi or their phytotoxic compounds on cytosolic E_{GSH}.

While transgenic sensor lines in the model dicotyledon *A. thaliana* have been in use for more than a decade, progress in other genetically accessible model plants has only recently started to gain momentum (Kirschner *et al.*, 2018; Müller-Schüssele *et al.*, 2020; Hipsch *et al.*, 2021; Giridhar *et al.*, 2022). To start filling this gap in temperate cereal crops, we created transgenic barley lines expressing the genetically encoded redox biosensor cytosolic Grx1–roGFP2 for E_{GSH}. We aimed to investigate stress resilience in barley and to monitor E_{GSH}

changes in different tissues *in vivo*. Herein, we characterize the obtained sensor lines and expose them to different abiotic and biotic stress treatments, revealing remarkable robustness of the cytosolic E_{GSH} in barley under abiotic stress, compared with high lability after exposure to the secretome of the necrotrophic fungus *B. cinerea*.

Materials and methods

Plant materials and growth conditions

Experiments were conducted in 'Golden Promise Fast', the *Ppd-H1* introgression line of the transformable barley (*Hordeum vulgare* L.) cultivar Golden Promise (Gol *et al.*, 2021; Amanda *et al.*, 2022). After 3 d of stratification at 4 °C on wet filter paper, seeds were transferred to germination paper (Anchor Paper Co., St. Louis, MO, USA). Barley was grown for up to 7 d in germination paper rolls with half-strength Hoagland solution (Hoagland and Arnon, 1938). Stress treatments were carried out as described in Osthoff *et al.* (2019) with 3 d of growth in half-strength Hoagland solution before transfer to nutrient solution with 150 mM NaCl and −0.8 MPa water potential [adjusted with polyethylene glycol (PEG) 8000]. Paper rolls were grown upright in a beaker in a climate cabinet under 16 h light (120 µmol photons m^{-2} s^{-1}) at 22 °C and 8 h dark at 18 °C.

For propagation and seed production, 7- to 10-day-old barley seedlings were transferred to the greenhouse and soil-grown with 15 h of light (1000–6000 lux) at 22 °C and 9 h of dark at 18 °C.

Generation of barley Grx1–roGFP2 lines

A barley-compatible expression vector for Grx1–roGFP2 was constructed by restriction enzyme-based cloning in the binary vector p6i-2x35s-TE9, kindly provided by Jochen Kumlehn (Himmelbach *et al.*, 2007), along with the pUBI-ABM (Watanabe *et al.*, 2016), as the source of the maize (*Zea mays* L.) ubiquitin promoter *ZmUbi1* and the *nos* terminator. A Grx1–roGFP2 fragment with *Bam*HI and *Sal*I restriction sites was ligated into the linearized UBIp-ABM (*Bam*HI, *Sal*I) with the ClonJet kit (ThermoFisher), to produce pZmUBI1pro-Grx1roGFP2-nosT. The ZmUBI1pro-Grx1roGFP2-nosT cassette was released by digestion with *Sfi*I and ligated into binary vector p6i-d35STE9 previously cut with the same enzyme. The resulting expression plasmid was transformed in Golden Promise Fast as described in Amanda *et al.* (2022), and T_0 hemizygous regenerants from eight independent events were produced. We screened the T_1 progenies from five out of the eight independent events for roGFP2 fluorescence with a confocal laser scanning microscope, and selected lines with 3:1 segregation of positive:negative fluorescence. T_2 progenies of positive fluorescent plants were further screened for 100% fluorescence expression to obtain homozygous transgenics. This procedure resulted in selecting two independent lines (5-3#39 and 2-1#1). We conducted all reported experiments in homozygous T_3 progenies of these lines.

Excitation scan of young barley leaves

Leaf discs were transferred into the wells of a 96-well plate containing 200 µl of imaging buffer (10 mM MES, 5 mM KCl, 10 mM $CaCl_2$, 10 mM $MgCl_2$ pH 5.8). For reduction and oxidation of Grx1–roGFP2, the imaging buffer was supplemented with 1.5 M H_2O_2, 5 mM 2,2'-dipyridyl disulfide (DPS), or 10 mM DTT to obtain total oxidation or reduction of the sensor. Leaf discs were vacuum infiltrated for 10 min and further incubated for 30 min. Fluorescence spectra were recorded with a plate reader (Clariostar®, BMG) with excitation wavelengths from 386 nm to 495 nm and emission set to 530–40 nm. Fluorescence was normalized over the fluorescence intensity at the isosbestic point (IP) of roGFP2 at 425 nm.

Confocal laser scanning microscopy of Grx1–roGFP2

Confocal laser scanning microscopy of Grx1–roGFP2 in barley roots and leaves was conducted with a LSM780 (Axio Observer.Z1, Carl Zeiss, Oberkochen, Germany) using a ×25 (Plan-Apochromat ×25/0.8) or ×40 (C-Apochromat ×40/1.2 W) objective by exciting roGFP2 at 405 nm (diode laser, 3%) and 488 nm (argon laser, 1.5%) and collecting roGFP2 fluorescence between 508 nm and 535 nm. Autofluorescence was detected at 430–470 nm after excitation at 405 nm. For Grx1–roGFP2 calibration, tissue samples were infiltrated by hand under pressure in a syringe and subsequently incubated for 15–20 min in imaging buffer containing 1.5 M H_2O_2, 5 mM DPS, or 10 mM DTT to obtain complete oxidation or reduction. Ratio calculations and further image analysis was performed in a MATLAB-based ratio software (RRA) (Fricker, 2016). Where indicated, regions of interest (ROIs) were set to nuclei as shown in Supplementary Fig. S1. The oxidation degree of roGFP2 (OxD) was calculated according to Schwarzländer *et al.* (2008).

Infection of barley leaves with B. cinerea

Leaves of 5-week-old barley plants were cut and inoculated with 10 µl of a suspension of *B. cinerea* conidia harvested from a 10-day-old sporulating malt extract agar plate, adjusted to 4×10^5 conidia ml^{-1}. The leaves were kept at ambient light in a humid chamber at 22 °C.

B. cinerea *secretome assay and ratiometric measurements of Grx1–roGFP2 in barley leaf discs*

To obtain an *in planta* secretome of *B. cinerea*, detached leaves of tomato were inoculated with 20 µl droplets with 10^5 conidia ml^{-1} in GB5 minimal medium. The secretome was obtained as described in Leisen *et al.* (2022), namely by collection and sterile filtration of the inoculation droplets from the leaves 48 h after inoculation, when expanding lesions had started to form. This solution contained mostly secreted *B. cinerea* proteins and both secreted and cytosolic plant proteins (Müller *et al.*, 2018), and was found to be highly phytotoxic (Leisen *et al.*, 2022). To remove salts from the GB5 medium used for inoculation and other low molecular weight compounds, the secretome was subjected to ultrafiltration, using Amicon® Ultra-4 centrifugal filter units with a molecular weight cut-off of 10 kDa. Protein concentration of the retentate was determined, and the solution adjusted to 8 µg ml^{-1} which causes necrosis when infiltrated into leaf tissue (Leisen *et al.*, 2022).

Leaf discs were punched from 5-week-old *H. vulgare* leaves, with a 7 mm cork borer. The leaf discs were floated on imaging buffer (10 mM MES, 5 mM KCl, 10 mM $CaCl_2$, 10 mM $MgCl_2$ pH 5.8) overnight in the dark in a 6-well plate. Subsequently, the leaf discs were transferred into the wells of a clear 96-well plate (containing 200 µl of imaging buffer) and gently pushed to the bottom of the well, with the adaxial side facing down. The plate was incubated in the dark for 1 h, then the buffer was replaced and the plate transferred into the plate reader (Clariostar®, BMG). A time series of fluorescence intensity measurements with sequential excitation at 400 ± 5 nm and 482 ± 8 nm, with the emission detected at 530 ± 20 nm was started. After three cycles, the measurement was paused, and the imaging buffer was replaced with imaging buffer containing 8 µg ml^{-1} *B. cinerea* filtered secretome. For reduction and oxidation of Grx1–roGFP2, the buffer was supplemented with 10 mM DTT or 5 mM DPS. For a control without treatment, the imaging buffer was replaced with fresh imaging buffer. The 96-well plate was transferred into a desiccator for 10 min vacuum infiltration. After infiltration with medium, the measurement was continued for a total time of 24.6 h.

After the plate reader run, the leaf discs were extracted from the 96-well plate and stored in deionized water. The leaf discs were transferred into imaging buffer with 50 μM propidium iodide (PI), vacuum-infiltrated for 10 min in a desiccator, and then washed with deionized water. Fluorescence was imaged using a stereomicroscope (Leica M205FCA) after excitation at 450–490 nm and emission at 500–550 nm wavelengths (GFP) and after excitation at 540–580 nm and emission at 593–667 nm (PI).

Glutathione detection in barley roots

After 96 h of stress treatment (see above), roots were incubated in 100 μM MCB (monochlorobimane) for exactly 30 min to label glutathione, and subsequently transferred to a 50 μM PI solution for 5 min to label cell walls and test for cell viability (Meyer *et al.*, 2001). After the labelling procedure, residual dye was washed out in deionized water. Fluorescence was imaged after excitation at 405 nm with emission wavelengths of 449–613 nm (MCB) and after 543 nm excitation with emission wavelengths of 613–704 nm (PI). Confocal z-stacks were taken with identical settings with the confocal laser scanning microscope covering 270 μm of root tissue in 10 μm slices per image. Gain and laser settings were kept constant throughout the imaging process. Only roots showing no severe cell damage indicated by PI staining were further analysed in ImageJ as 8-bit images of maximum intensity projections of the z-stacks. The mean pixel intensity was extracted of the area of the root tip in each image and blotted as a boxplot using GraphPad Prism 9.

Glutathione reductase activity assay in barley root extracts

Flash-frozen and pulverized [TissueLyser (Qiagen) for 1.5 min, 30 Hz] root material was dissolved in 100 μl of 100 mM K_2HPO_4/KH_2PO_4 at pH 7.5 supplemented with 0.5 mM EDTA and 0.1% of plant protease inhibitor cocktail P9599 (Sigma). Samples were vortexed and centrifuged at 20 000 *g* for 5 min at 4 °C. The supernatant was transferred into a new tube and the centrifugation step was repeated. Protein concentration was determined in a Bradford assay (Bradford, 1976). Extract containing 5 μg of protein was used in a total assay volume of 250 μl for the DTNB [5,5′-dithiobis(2-nitrobenzoic acid)]-based GR activity assay (Smith *et al.*, 1988; Marty *et al.*, 2009), together with 1 mM EDTA, 750 μM DTNB, 1 mM GSSG in 100 mM K_2HPO_4/KH_2PO_4 at pH 7.5. TNB absorbance was followed at 412 nm using a plate reader (Clariostar®, BMG). After 5 min of measuring background activity, NADPH was added to a final concentration of 200 μM. GR activity was calculated via the increase of $A_{412\ nm}$ min^{-1} and the molar extinction coefficient of TNB.

Results

Generation of stable barley lines expressing cytosolic Grx1–roGFP2

We generated barley (cv. Golden Promise Fast) lines constitutively expressing Grx1–roGFP2 under the control of the maize ubiquitin promotor (*ZmUbi*), including the 5'-untranslated region (UTR) intron. Two independent lines originating from shoots from different calli were chosen based on consistent GFP fluorescence (5-3 #39 and 2-1 #1) and brought to homozygosity. In the chosen homozygous lines, we observed Grx1–roGFP2 signal, independent of tissue type or developmental stage (Fig. 1). No phenotypic difference in growth was observed between barley expressing the sensor and the Golden Promise Fast background.

The epidermal layer of barley leaves showed the typical sensor fluorescence signal in the nucleus and cytosol (Fig. 1A). High autofluorescence signal was detected after excitation at 405 nm in guard cells and in vacuoles of mesophyll cells, as well as in the wall of root cells (Fig. 1A; Supplementary Fig. S1A–C).

Cytosolic Grx1–roGFP2 reacts to oxidizing and reducing agents in barley shoots and roots

To assess if the sensor is responsive to exogenously induced reduction or oxidation, leaf discs of 7-day-old barley plants were exposed to reducing and oxidizing agents. We observed a roGFP2-typical *in planta* excitation spectrum after excitation of the leaf discs at 386–495 nm (Fig. 1B). Reduction of the sensor with DTT led to a higher excitation peak, while oxidation with H_2O_2 or DPS led to a lower excitation peak in the spectral range above the IP at 425 nm. Below the IP, the influence of sensor oxidation or reduction on *in vivo* excitation spectra was only low, resulting in a minor contribution to 405/488 ratio changes. The *in vivo* spectroscopic dynamic range (δ) of Grx1–roGFP2 was calculated to be ~2- to -3-fold (405/488) (×2.79, 2-1 #1; ×2.65, 5-3 #39). Untreated barley leaves showed a similar spectral signal to the DTT-treated leaves, suggesting a largely reduced sensor under physiological conditions. Furthermore, the sensor did not behave significantly differently between the two independent lines (Fig. 1B; Supplementary Fig. S1D).

Since Grx1–roGFP2 is diffusing freely between the cytosol and nucleus (Schwarzländer *et al.*, 2016), we employed nuclear ROIs for quantification of microscopic sensor readout to reduce autofluorescence interference from the cell wall or vacuole (Supplementary Fig. S1B, C). Using nuclear ROIs, we further determined the *in vivo* dynamic range of Grx1–roGFP2 in barley plants based on confocal microscopy (Fig. 2; Supplementary Figs S2–S4). To reach full sensor oxidation, the addition of at least 1 M exogenous H_2O_2 was necessary (Supplementary Fig. S3). We calibrated Grx1–roGFP2 in root and leaf tissue of young barley seedlings and observed tissue-dependent differences (Fig. 2; Supplementary Fig. S2). While the calibration of line 5-3 #39 and line 2-1 #1 in leaves resulted in a dynamic range of δ=1.3–1.5, calibration of the root tissue resulted in a dynamic range of δ=2.3–2.7 depending on the oxidizing agent used. Furthermore, the physiological state of Grx1–roGFP2 in roots revealed a higher 405/488 nm ratio of 0.93 ± 0.50 (2-1 #1) and 1.05 ± 0.61 (5-3 #39) compared with leaves with a ratio of 0.63 ± 0.27 (2-1 #1) and 0.60 ± 0.18 (5-3 #39), suggesting a slightly more oxidized sensor in roots than in leaves.

Cytosolic E_{GSH} reacts only slowly and mildly to severe growth-impairing osmotic and salt stress

A recent transcriptomic study (Osthoff *et al.*, 2019) showed that barley seedlings treated with a combination of salt and osmotic stress in a paper roll system up-regulate transcript encoding the

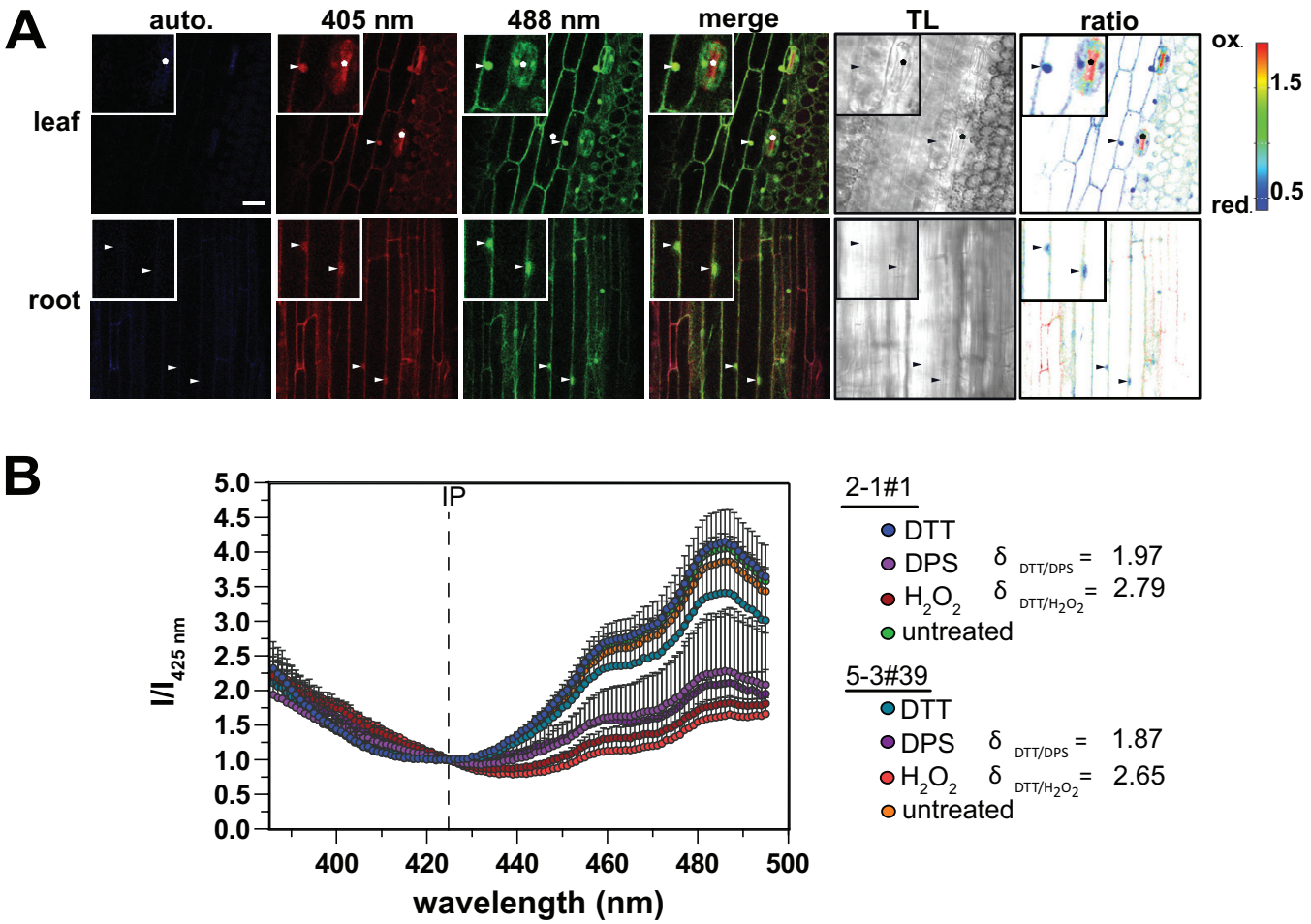

Fig. 1. Grx1–roGFP2 expression in barley leaf and root tissue. (A) Confocal microscopy images of roGFP2 (405 nm and 488 nm excitation; 508–535 nm emission) and autofluorescence (auto, 405 nm excitation; 430–470 nm emission). The merge image displays the overlay of 405 and 488 intensities. TL, transmitted light. Arrowheads indicate nucleus-localized sensor signal, and the asterisks show regions of high autofluorescence. Scale bar=40 µm. (B) Excitation scan (386–495 nm; emission: 530–40 nm) of barley leaf discs untreated and treated with 10 mM DTT, 5 mM DPS, or 1.5 M H_2O_2 (see also Supplementary Fig. S1 for spectra of untreated plant lines only). Fluorescence was normalized over the fluorescence intensity at the isosbestic point (IP) of roGFP2 at 425 nm. Significance between genotypes and treatments of the 405 nm and 488 nm peak intensity was tested with a two-way ANOVA and Tukey's post-hoc test with $\alpha<0.05$. No significant differences were observed between the lines within one treatment, while peak intensities of 488 nm were significantly different in reducing (DTT) and oxidizing (H_2O_2 and DPS) treatments.

cytosolic isoform of GR (GR1; HORVU6Hr1G089780) after 24 h of stress exposure. As the expression of this major enzyme for maintaining a highly reduced cytosolic glutathione redox status was affected under these conditions and the used paper roll system allows for soil-free imaging of barley plants, we chose the same experimental conditions for barley expressing Grx1–roGFP2 to assess potential effects of this stress treatment on the cytosolic E_{GSH}.

As reported by Osthoff *et al.* (2019), barley seedlings treated with a combined stress of 150 mM NaCl and a water potential of –0.8 MPa (adjusted using PEG8000) showed a decrease in root growth (Fig. 3). While the mean root growth of barley grown for 7 d in half-strength Hoagland solution showed root lengths of 57.47 ± 22.05 mm (mean of 5-3 #39 and 2-1 #1, control), root growth decreased significantly after a combined salt and osmotic stress for 96 h to 34.7 ± 14.81 mm (mean of 5-3 #39 and 2-1 #1, 150 mM NaCl, –0.8 MPa PEG8000).

Next, we followed the redox state of the Grx1–roGFP2 sensor in roots at 24, 48, and 96 h after the start of the stress (Osthoff *et al.*, 2019). The disulfide of roGFP2 has a consensus midpoint potential of –280 mV at pH 7 and is thus particularly suited to track oxidative changes to the E_{GSH} in the cytosol which has been determined to be –310 mV (pH 7) or less in *A. thaliana* (reviewed in Müller-Schüssele *et al.*, 2021b). Grx1–roGFP2 redox state was read out via confocal laser scanning microscopy and quantified via ratio image analysis of nuclei as ROIs. We found that cytosolic E_{GSH} is maintained during the first 48 h of stress treatment. After 96 h, we observed a significant but small oxidative shift in the 405/488 nm ratio between stressed (1.05) and non-stressed (0.86) plants (Fig. 4;

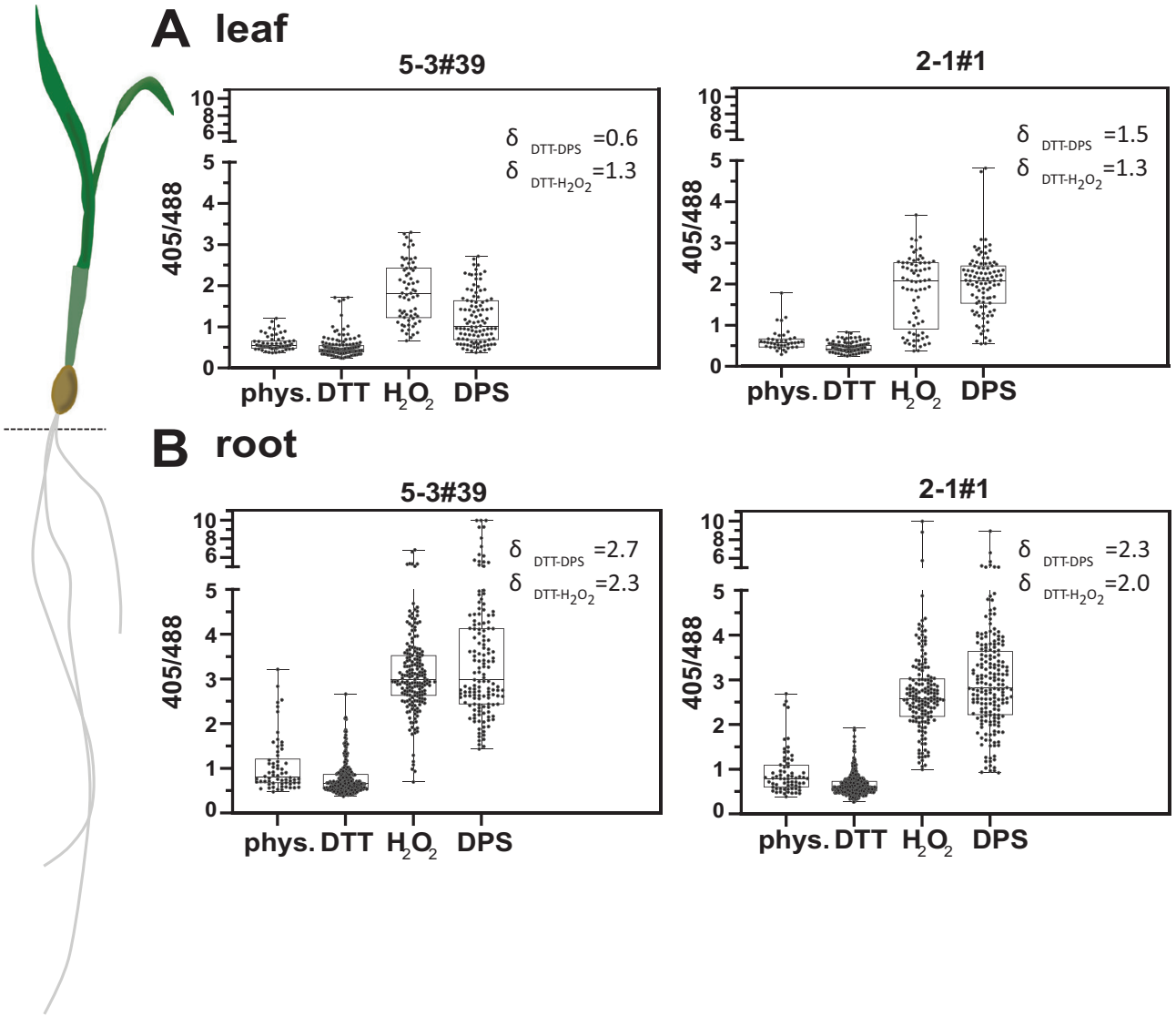

Fig. 2. Grx1–roGFP2 sensor calibration in barley leaf and root tissue. Box plots of Grx1–roGFP2 signal ratios (405/488) calculated from fluorescence intensities in nuclei of leaf (A) and root (B) tissue treated with 10 mM DTT, 5 mM DPS, 1.5 M H_2O_2, or imaging buffer (phys.=physiological conditions) and imaged via confocal microscopy. A one-way ANOVA and Tukey's multiple comparison test were conducted on log-transformed ratio values. Significantly different treatments (P<0.0001) are indicated by different letters. Boxes display 25–75 percentiles, with whiskers showing min to max values. The middle line indicates the median, and dots represent the data of every nucleus obtained from 2–5 seedlings per treatment.

Supplementary Figs S5–S7). The measured difference in the 405/488 nm ratio corresponds to only a 3% shift in degree of sensor oxidation.

Investigating the molecular basis for E_{GSH} robustness under abiotic stress

According to the Nernst equation, E_{GSH} is dependent on both the total concentration of GSH and the proportion of GSSG. Thus, a less negative local E_{GSH} as measured via roGFP2 redox state could be caused by either increased GSSG levels or decreased total glutathione content in the cytosol. GR recycles GSSG back to GSH, using NADPH as electron donor. As the K_m of this important enzyme is in the nanomolar range, [GSSG] would only rise if the enzymatic capacity of GR is not sufficient to reduce GSSG immediately or if there is a shortage of NADPH. Transcriptomic analyses of Osthoff *et al.* (2019) identified the transcripts of both barley GR isoforms as differentially up-regulated after 24 h of combined salt and osmotic stress [GR1, HORVU6Hr1G089780 $\log_2$fold change (FC) 1.3; GR2, HORVU4Hr1G073930 $\log_2$FC 1.5]. In contrast, transcripts encoding barley orthologues of the two proteins involved in GSH biosynthesis (GSH1 HORVU1Hr1G015590 and GSH2 HORVU5Hr1G027100) were not differentially expressed under those conditions (Osthoff *et al.*, 2019).

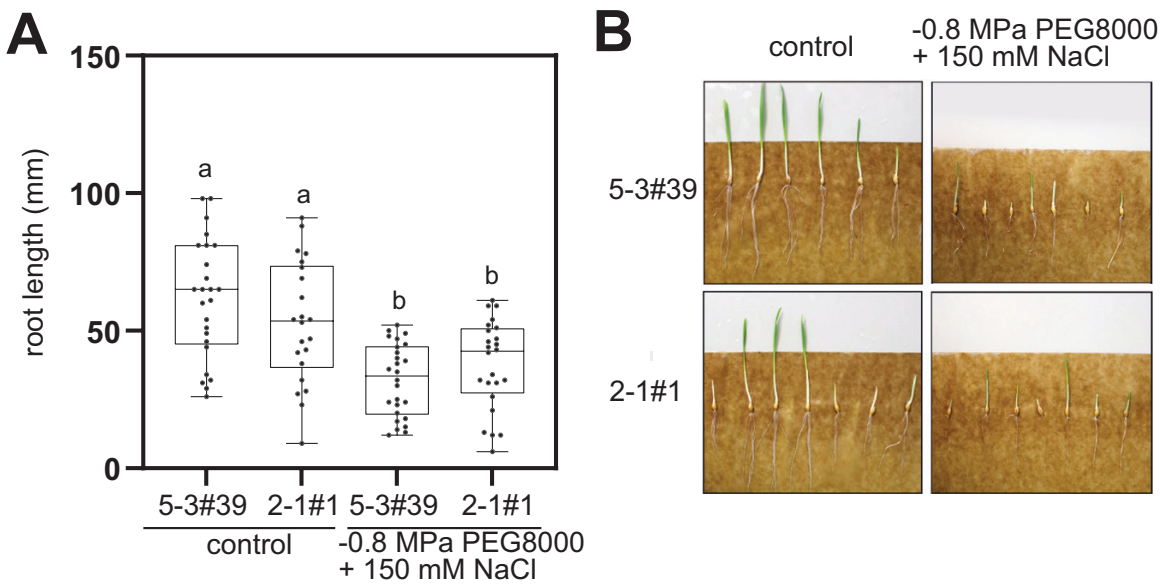

Fig. 3. Effect of combined osmotic and salt stress on barley seedling root growth. (A) Root length of 7-day-old barley plants after 96 h of combined osmotic and salt stress. Boxes display 25–75 percentiles, with whiskers showing min to max values. The median is indicated by the horizontal line. Dots show individual root lengths measured of 21–26 individual seedlings. (B) Example images of Grx1–roGFP2 sensor lines under control and stress conditions, 96 h after the beginning of the stress.

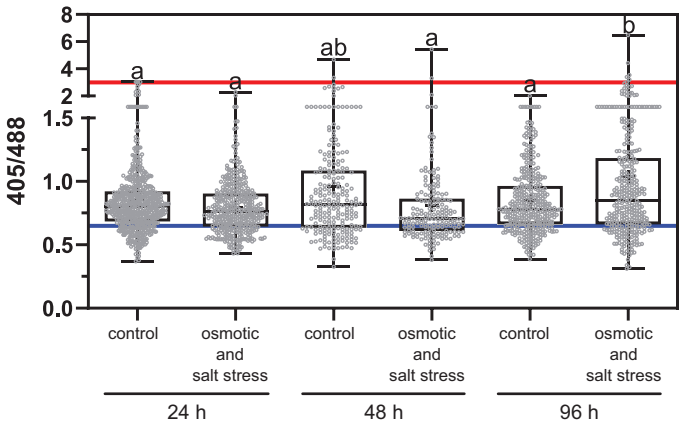

Fig. 4. roGFP2 405/488 ratio in roots of barley seedlings after 24, 48, or 96 h of combined osmotic and salt stress (150 mM NaCl, 0.8 MPa PEG8000). Box plots including raw data points of roGFP2 nuclear signal ratios (405/488). Boxes display 25–75 percentiles, with whiskers showing min to max values. The median is displayed as a horizontal line, and the mean is indicated with the '+' sign. Lines indicate 100% oxidation (red) and reduction (blue) of the sensor (according to means of calibration with line 2-1 #1 root values, see Fig. 2). Two-way ANOVA was conducted on log-transformed ratio values, with different letters indicating significant differences according to Tukey's multiple comparisons test (P<0.0001). Between 170 and 256 nuclei were analysed from 3–5 seedlings per treatment and time point.

Thus, we used an enzymatic assay for GR activity in plant extracts to test if total GR activity is increased in response to the same stress treatment. We did not find significantly reduced or increased total GR activity in the 96 h stress treatment samples (Fig. 5A). The GR activity of the 2-1 #1 line under control and stress conditions remained constant, with values of 105.5 ± 36.4 nmol TNB min^{-1} mg^{-1} protein and 105.9 ± 39.8 nmol TNB min^{-1} mg^{-1} protein, similar to the 5-3 #39 line with a slightly lower measured GR activity of 98.9 ± 46.7 nmol TNB min^{-1} mg^{-1} protein and 92.3 ± 43 nmol nmol TNB min^{-1} mg^{-1} protein. To compensate for possible differences in the individual measurements, we normalized the measured activities after stress treatment with those of the corresponding control treatment (Fig. 5B). The resulting normalized ratio values of 1.1 ± 0.5 (2-1 #1) and 1.0 ± 0.6 (5-3 #39) did not show significant differences in response to the stress treatment and maintained a high variance.

We additionally tested if the stress treatment modifies the total glutathione content after 96 h (Fig. 5C, D). We stained intact root tips with MCB, a GSH-specific dye that becomes fluorescent after glutathione *S*-transferase conjugates it to GSH [emitting fluorescence at 449–613 nm after excitation at 405 nm (Haugland *et al.*, 1996)]. MCB-stained roots of stressed (150 mM NaCl, –0.8 MPa PEG8000, 96 h) and unstressed seedlings were imaged with a confocal laser scanning microscope. We did not find significantly different staining intensities between control and stress samples (Fig. 5C, D), excluding a major change in glutathione content after stress treatment.

Cells bordering Botrytis cinerea*-induced leaf lesions only sporadically display oxidized cytosolic* E_{GSH}

As we did not observe E_{GSH} oxidation under severe abiotic stress conditions, we tested if biotic stress caused by a necrotrophic

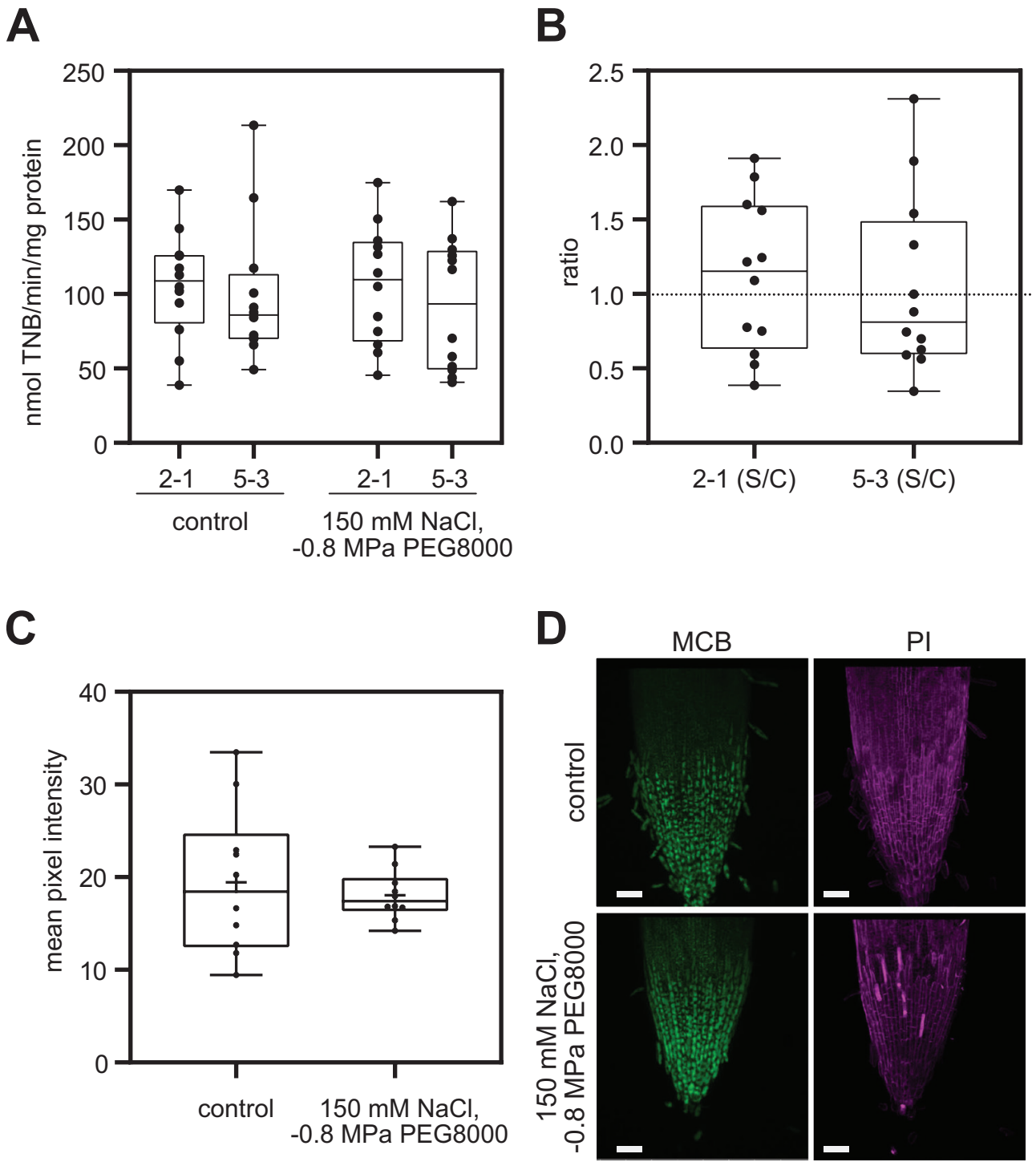

Fig. 5. DTNB-based glutathione reductase assay (A, B) and detection of total glutathione via MCB labelling (C, D) in barley roots after 96 h osmotic and salt stress. (A) Absolute GR activity under control and 96 h of stress conditions displayed as box plots, with boxes displaying 25–75 percentiles and whiskers showing min to max. Median is shown as a horizontal line. Individual GR activities of 12 biological replicates for each line and condition are shown as dots. (B) GR activity in stressed samples (S) was divided by the corresponding control activity (C). A two-way ANOVA (A) and *t*-test (B) were conducted on datasets A and B with α=0.05, and no significant differences were observed. (C) Mean pixel intensities of unstressed and stressed (150 mM NaCl, –0.8 MPa PEG8000) wild-type barley root tips stained with MCB were extracted with ImageJ (8-bit, 0–255 display range). Boxes display 25–75 percentiles, with whiskers showing min to max values; the median is displayed as a constant line. The mean of all data points is shown as '+' (n=10). No significant differences were detected (*t*-test). (D) Example of maximum intensity projection of wild-type barley root tips (see C) stained with MCB (excitation, 405 nm; emission, 449–613 nm) and PI (excitation, 543 nm; emission, 613–704 nm). Scale bar=100 µm.

fungus would lead to E_{GSH} oxidation. We chose *B. cinerea*, that has a broad range of host plants and is believed to kill host cells by triggering a strong oxidative burst and hypersensitivity response-induced programmed cell death before colonizing the dead plant tissue (Bi *et al.*, 2023). We were able to infect *H. vulgare* leaves using droplet infection with *B. cinerea* conidia on cut leaves and observed formation of necrotic lesions after 2–3 d (Fig. 6A). Inspecting the living cells surrounding the lesions using confocal microscopy, we found increased overall autofluorescence after excitation at 405 nm, that was also present in distinct subcellular foci in living cells next to lesions (Supplementary Fig. S8). Unexpectedly, Grx1–roGFP2 sensor read-out still showed a largely reduced state, compared with the calibration conducted in the same material (Supplementary Fig. S8). Interestingly, only few and single cells showed a potential oxidation of Grx1–roGFP2 (Fig. 6A; Supplementary Fig. S8). We hypothesize that cell death, possibly preceded by oxidation of the cytosol, occurred asynchronously and during a relatively short time interval during spreading of lesions. To synchronize the effect of secreted fungal effectors on leaf cells, we developed a system to track the sensor redox state in a plate reader-based setup, using filtered *B. cinerea* secretome.

Filtered secretome of Botrytis cinerea *causes cell damage and* E_{GSH} *oxidation in barley*

Botrytis cinerea secretes a complex mixture of phytotoxic proteins during infection. We reasoned that simultaneous treatment of leaf tissue with these proteins would result in a more consistent synchronized oxidative response of cells. Proteins of the phytotoxic secretome of *B. cinerea* were obtained by collecting inoculation droplets from detached tomato leaves showing expanding necrosis 2 d after inoculation, sterile filtration to remove infectious conidia, and size filtration for proteins >10 kDa (see the Materials and methods). *Hordeum vulgare* leaf discs infiltrated with this secretome fraction (8 µg ml^{-1}) showed complete oxidation of Grx1–roGFP2 within 12–24 h, compared with control samples infiltrated with buffer (Fig. 6B; see Supplementary Fig. S9 for raw data including WT autofluorescence and Supplementary Fig. S10 for sensor ratio data). This oxidation started almost immediately after the addition of secretome, before cell death, and thereby loss of Grx1–roGFP2 sensor signal was observed. As a complementary read-out, we removed leaf discs from the plate reader-based setup after 20 h with or without secretome infiltration and assessed Grx1–roGFP2 redox state in nuclear ROIs, confirming specific sensor oxidation on the microscopic level (Supplementary Fig. S11). After the plate reader run (Fig. 6B), leaf discs were stained with PI to test for secretome-induced cell damage. PI signal was read out with a fluorescence stereomicroscope and revealed stained nuclei in leaf areas, indicating damaged or dead cells, similar to a boiled tissue control. In PI-stained cells, GFP signals were generally low or absent (Fig. 6C; Supplementary Fig. S12), confirming profound cell damage or cell death.

Discussion

In this study we generated and characterized two independent transgenic barley (*H. vulgare*, cv. Golden Promise Fast) lines expressing the genetically encoded biosensor Grx1–roGFP2 under the control of the *Z. mays* ubiquitin promoter including the 5' UTR intron (Christensen and Quail, 1996). As expected, the biosensor was constitutively expressed and localized to the cytosol and nucleus. The fluorescence intensity was sufficiently high for ratiometric sensor read-out in all examined tissues. As we observed high autofluorescence after excitation with UV light (405 nm) in the apoplast and sometimes the vacuole and cell walls, we preferably calculated 405/488 nm ratios from ROIs set to nuclei. Using this approach, we determined that the *in vivo* dynamic range of cytosolic Grx1–roGFP is ~1.3–1.5 in leaves and ~2.3–2.7 in roots. The previously reported *in vitro* dynamic range of roGFP2 was ~8.2–9.2 (405/488 nm) (Schwarzländer *et al.*, 2008; Aller *et al.*, 2013) while *in vivo* samples often displayed decreased dynamic ranges of ~5 in confocal microscopy or ~3 in plate reader-based sensor read-out in *A. thaliana* (Ugalde *et al.*, 2021, 2022). This difference in dynamic range between *in vitro* and *in vivo* sensor read-out can be explained by interference of plant compounds that overlay the changes in sensor absorption in the UV range (below the IP at ~425 nm). This is also the case for barley, where the change in roGFP2 excitation in the UV range between fully reduced and fully oxidized plant samples is very small (Fig. 1B). Thus, the 405/488 sensor ratio displays a lower dynamic range *in vivo* than *in vitro*. The observed differences in calibration between leaf samples and root samples (Fig. 2) could be attributed to insufficient penetration of the oxidants H_2O_2 and DPS into barley leaves. However, within each tissue, sensor oxidation caused by 1.5 M H_2O_2 or 5 mM DPS was not significantly different. Usually, lower concentrations of H_2O_2 (10–100 mM) are used for *in vivo* roGFP2 sensor calibration but were not effective in barley (this study; Supplementary Fig. S3) and potato (Hipsch *et al.*, 2021). Generally, it is very important to identify the optimal conditions for sensor calibration that allow determination of the 405/488 nm ratio values for both 0% and 100% roGFP oxidation (OxD), especially when milliVolt values for the glutathione redox potential are to be calculated (reviewed in Müller-Schüssele *et al.*, 2021b). Using the sensor calibration in roots and the untreated (physiological) root samples, we calculated that the cytosolic E_{GSH} of the barley cytosol is approximately –308 mV to –320 mV assuming a pH of 7.2 (Supplementary Fig. S2). This is close to the cytosolic E_{GSH} in *A. thaliana*, which was measured as approximately –320 mV to –310 mV (Meyer *et al.*, 2007; Schwarzländer *et al.*, 2008; Aller *et al.*, 2013). This E_{GSH} in the barley cytosol results in mostly

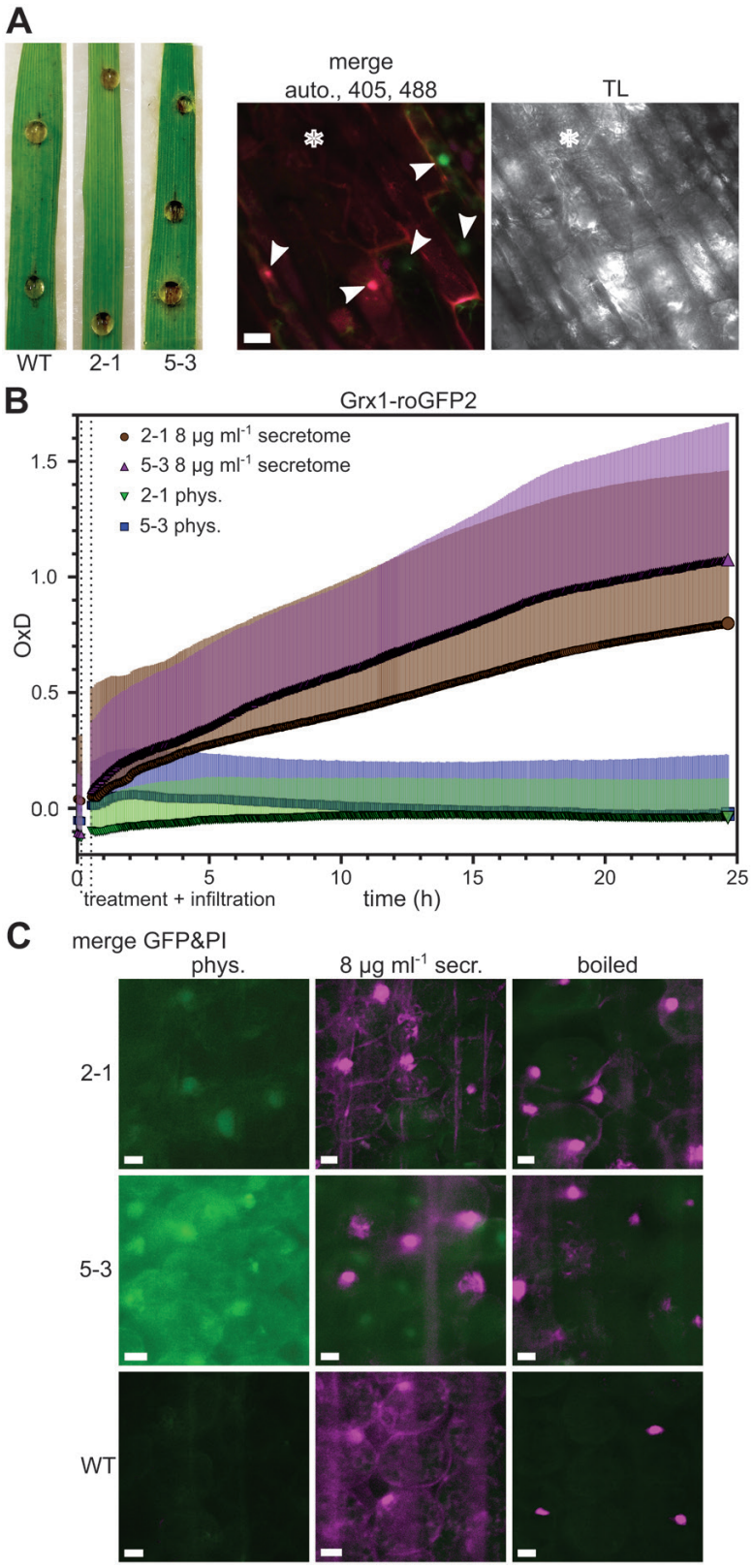

Fig. 6. Effect of *Botrytis cinerea*-induced damage on cytosolic redox potential. (A) Exemplary leaves of *H. vulgare* Golden Promise Fast (WT) and Grx1–roGFP2-expressing lines 2-1 and 5-3 after 2–3 d infection with *B. cinerea* (left panel). Confocal microscopy of living cells next to *B. cinerea*-induced necrotic lesions [merge image of autofluorescence after excitation at 405 nm (auto.), 405 nm excitation of roGFP2, and 488 nm excitation of roGFP2

as well as transmitted light (TL)]. The asterisk indicates the area covered in fungal hyphae. Arrowheads point to nuclear sensor signals, with magenta indicating oxidation and green indicating reduction. See Supplementary Fig. S7 for additional data and individual channel images. Scale bar=20 µm. (B) Grx1–roGFP2 response in leaf discs of 5-week-old *H. vulgare* treated with 8 µg ml^{-1} *B. cinerea* filtered secretome: oxidation degree (OxD) of cytosolic Grx1–roGFP2 over time with two independent lines (n=5; error bars, ±SD; sequential excitation 430 ± 5 nm and 482 ± 8 nm; emission 530 ± 20 nm). (C) Qualitative assessment of cell damage in *H. vulgare* leaf discs shown in (B) [after 24.6 h of infiltration with *B. cinerea* filtered secretome (8 µg ml^{-1} secr.) or buffer (phys.)], by staining with PI (magenta). Boiling (10 min 60 °C) served as an additional positive control for cell damage. All presented images are merges of the PI and GFP fluorescence channels, taken with a fluorescence binocular (PI excitation 540–580 nm, emission 593–667 nm; GFP excitation 450–490 nm, emission 500–550 nm). Magnification: 320-fold; scale bars=10 µm.

reduced Grx1–roGFP2, supporting the suitability of Grx1–roGFP2 to sense oxidative changes in this compartment.

We also observed a small, but statistically significant difference in the 405/488 nm sensor ratio between barley roots and leaves (Fig. 2; Supplementary Fig. S2), which suggests a slightly more reduced physiological steady state of Grx1–roGFP2 in leaves than in roots, corresponding to a 5–10 mV difference. However, we cannot rule out that the read-out of roGFP2 excitation ratios differs slightly between these organs due to tissue-specific differences in wavelength penetration or autofluorescence.

Many molecules in plants emit fluorescence after excitation in the UV range such as chlorophyll, lignin, or alkaloids (Donaldson, 2020). We detected high levels of autofluorescence in barley leaves and roots excited with 405 nm. Since cells may contain multiple autofluorescent compounds, we cannot narrow down the exact source of autofluorescence in these tissues after excitation with 405 nm. Barley tissues are rich in phenolic compounds such as the phenylpropanoid ferulic acid (4-hydroxy-3-methoxy-cinnamicacid) with concentrations ranging from 359 µg to 624 µg g^{-1} DW (Hernanz *et al.*, 2001; Bonoli *et al.*, 2004).

By applying stress to the generated reporter lines, we observed shorter seminal root lengths after 96 h (4 d) of combined salt and osmotic stress comparable with Osthoff *et al.* (2019). We therefore used this time point to assess shifts in the cytosolic glutathione redox potential. We first monitored the roGFP2 redox state 24, 48, and 96 h after combined stress treatment and were able to detect significant but small changes in the roGFP2 oxidation degree after 96 h. The measured shift in roGFP2 405/488 nm ratio corresponds to a 3% shift in degree of oxidation, implying a +2.1 mV shift from –314 mV (control 96 h) to –311.9 mV (150 mM NaCl, –0.8 MPa PEG8000) (pH 7.2, calibration values of 2-1 #1 root). We conclude that *H. vulgare* cytosolic E_{GSH} is robust, even if a stress-caused growth delay is already evident.

Water deficit and salt stress caused up-regulation of transcripts related to the response to an oxidative challenge (Osthoff *et al.*, 2019). Several enzymes involved in the response to oxidative stress draw electrons from the glutathione pool, generating local GSSG. The highest flux of electrons can arguably be expected from DHAR, which re-reduces dehydroascorbate to ascorbate in the ascorbate–glutathione cycle that scavenges H_2O_2 (Foyer and Noctor, 2011). As we detected only a slight oxidative response of Grx1–roGFP2 after 96 h of combined water deficit and salt stress, the cytosolic E_{GSH} in barley seems highly resilient against oxidative changes. Possible reasons could be that (i) GSH does not serve as electron donor to mitigate these stress conditions or (ii) GSH serves as electron donor and generates GSSG but compensatory mechanisms keep E_{GSH} constant. According to the Nernst equation, E_{GSH} could be kept constant via an increase in GSH or removal of GSSG. To test these scenarios, we assessed total glutathione content and total GR activity, but we found no changes in these parameters under the tested stress conditions. However, it should be noted that our imaging-based approach is limited regarding the investigated tissue type and that the enzyme activity-based approach can only assess total GR activity (i.e. GR1 and GR2). Thus, we cannot completely rule out an increase in activity of cytosolic GR1 under osmotic and salt stress. Another, untested possibility is an efficient export of GSSG from the cytosol, for example to the vacuole (Morgan *et al.*, 2013; Marty *et al.*, 2019).

We created our reporter lines in the transformable background Golden Promise Fast, which has shown resilience under drought stress (Gol *et al.*, 2021). Our lines in this background showed reductions in root growth under combined salt and osmotic stress, similarly to the German spring barley cultivar Scarlett (Osthoff *et al.*, 2019), indicating that Golden Promise Fast does respond to these abiotic stresses. However, it is formally possible that the robust redox state displayed by Golden Promise Fast under our combined stress treatments is a particularity of this genetic background. Thus, it may be of interest to introgress the reporter in other cultivars and study its response to similar stresses.

Exposing our reporter lines to the necrotrophic fungus *B. cinerea* revealed that most cells bordering 2- to 3-day-old necrotic lesions do not show oxidative shifts in E_{GSH}. This suggests that there is no zone with synchronized extensive oxidative damage around lesions, at least under the investigated experimental conditions. However, when sterile-filtered phytotoxic secretome (devoid of infectious material and cytotoxic metabolites) was simultaneously applied by infiltration into barley leaf discs, a continuously progressing, concerted oxidation of Grx1–roGFP2 was observed within the first day of exposure. The *B. cinerea* secretome, which contained only proteins >10 kDa after ultrafiltration, was applied in a similar concentration as the original secretome obtained from

inoculated tomato leaves after 48 h. These data indicate that the complex protein mixture in *B. cinerea* secretome is sufficient to induce a severe oxidative shift of the cytosolic E_{GSH} in barley. The secretome contains a mixture of cell wall-degrading enzymes, membrane pore-forming phytotoxic proteins (e.g. necrosis- and ethylene-inducing proteins), as well as several proteins inducing hypersensitive cell death by activation of pattern recognition receptors in the plant plasma membrane (Leisen *et al.*, 2022; Bi *et al.*, 2023). It will be interesting to investigate whether and how the overstimulation of cellular defence mechanisms and/or the impaired function of cellular reducing systems undermine the robustness of cytosolic E_{GSH} and are contributing to trigger plant cell death induced by *B. cinerea*. Our observations of 2- to 3-day-old lesions suggest that in a natural infection, oxidation of cytosolic E_{GSH} in bordering cells is occurring asynchronously in *H. vulgare*.

In general, the glutathione-dependent redox system is viewed as a house-keeping redox system and E_{GSH} as a relatively constant parameter in the plant cytosol. Given the robustness of E_{GSH}, it may be tempting to propose that this parameter could be a strong predictor of irreversible damage and imminent cell death. In this regard, E_{GSH} reporter lines would be interesting resources to screen for higher stress resilience or mechanisms of plant–pathogen interactions. To further dissect the causes and consequences of high robustness versus lability (stability of instability) of cytosolic E_{GSH} under different conditions, additional investigations using genetic analyses and tools will be required.

In conclusion, we generated barley reporter lines that allow monitoring of the cytosolic E_{GSH} via the Grx1–roGFP2 oxidation state and that can be used to further investigate abiotic and biotic stress tolerance in barley.

Supplementary data

The following supplementary data are available at *JXB* online.

Fig. S1. Screening and analysis of Grx1–roGFP2 signal in barley.

Fig. S2. Physiological glutathione redox potential as indicated by Grx1–roGFP2 in barely root and leaf tissue.

Fig. S3. Calibration of Grx1–roGFP2 with 0.1–1.5 M H_2O_2 in barley leaf tissue.

Fig. S4. Calibration of barley root and leaf tissue.

Fig. S5. Grx1–roGFP2 ratio after 24 h of combined stress treatment.

Fig. S6. Grx1–roGFP2 ratio after 48 h of combined stress treatment.

Fig. S7. Grx1–roGFP2 ratio after 96 h of combined stress treatment.

Fig. S8. Grx1–roGFP2 ratio in cells near *B. cinerea*-induced lesions.

Fig. S9. Raw data of fluorescence channel intensities after infiltration with *B. cinerea* secretome in a plate reader-based assay (Fig. 6B).

Fig. S10. Grx1–roGFP2 ratio after infiltration with *B. cinerea* filtered secretome.

Fig. S11. Grx1–roGFP2 ratio after infiltration with *B. cinerea* filtered secretome—complementary read-out by confocal microscopy.

Fig. S12. PI staining after infiltration with *B. cinerea* filtered secretome.

Acknowledgements

We thank Alexa Brox and Maria Homagk (Chemical Signalling, INRES, University of Bonn) for assistance in cloning, barley cultivation, and stress treatments, and Edelgard Wendeler (MPIPZ) for her technical support for the generation of the transgenic lines.

Author contributions

FB, MH, IA, AJM, and SJMS: design; FB, AK, HT, JI, and NS: performing experiments and data analysis; SJMS, MS, AJM, FH, and IA: supervision and providing resources; FB and SJMS: writing the manuscript with contributions from all authors. All authors approved the manuscript before submission.

Conflict of interest

The authors declare that they have no conflicts of interest.

Funding

This work was supported by Deutsche Forschungsgemeinschaft (DFG) (Research Training Group GRK2064: 'Water use efficiency and drought stress responses: From Arabidopsis to barley' (AJM, MS, FAB, and SJM) and FOR 5098 ICIPS (JI, SJM)), as well as the Max Planck Society (IFA). MH and SJM are grateful for funding obtained from BioComp 3.0 'Dynamic Membrane Processes in Biological Systems'.

Data availability

All data supporting the findings of this study are available within the paper and within its supplementary data published online. Raw data are available from the corresponding author, Stefanie Müller-Schüssele, upon request.

References

Aller I, Rouhier N, Meyer AJ. 2013. Development of roGFP2-derived redox probes for measurement of the glutathione redox potential in the cytosol of severely glutathione-deficient *rml1* seedlings. Frontiers in Plant Science **4**, 506.

Amanda D, Frey FP, Neumann U, *et al*. 2022. Auxin boosts energy generation pathways to fuel pollen maturation in barley. Current Biology **32**, 1811

Arnaud D, Deeks MJ, Smirnoff N. 2023. Organelle-targeted biosensors reveal distinct oxidative events during pattern-triggered immune responses. Plant Physiology **191**, 2551–2569.

Bangash SAK, Müller-Schüssele SJ, Solbach D, Jansen M, Fiorani F, Schwarzländer M, Kopriva S, Meyer AJ. 2019. Low-glutathione mutants are impaired in growth but do not show an increased sensitivity to moderate water deficit. PLoS One **14**, e0220589.

Bi K, Liang Y, Mengiste T, Sharon A. 2023. Killing softly: a roadmap of *Botrytis cinerea* pathogenicity. Trends in Plant Science **28**, 211–222.

Bonoli M, Marconi E, Caboni MF. 2004. Free and bound phenolic compounds in barley (*Hordeum vulgare* L.) flours. Journal of Chromatography A **1057**, 1–12.

Bradford MM. 1976. A rapid and sensitive method for the quantitation of microgram quantities of protein utilizing the principle of protein–dye binding. Analytical Biochemistry **72**, 248–254.

Chassot C, Buchala A, Schoonbeek H, Métraux J, Lamotte O. 2008. Wounding of Arabidopsis leaves causes a powerful but transient protection against Botrytis infection. The Plant Journal **55**, 555–567.

Christensen AH, Quail PH. 1996. Ubiquitin promoter-based vectors for high-level expression of selectable and/or screenable marker genes in monocotyledonous plants. Transgenic Research **5**, 213–218.

Dawson IK, Russell J, Powell W, Steffenson B, Thomas WTB, Waugh R. 2015. Barley: a translational model for adaptation to climate change. New Phytologist **206**, 913–931.

Donaldson L. 2020. Autofluorescence in plants. Molecules **25**, 2393.

Foyer CH, Noctor G. 2011. Ascorbate and glutathione: the heart of the redox hub. Plant Physiology **155**, 2–18.

Fricker MD. 2016. Quantitative redox imaging software. Antioxidants & Redox Signaling **24**, 752–762.

Giridhar M, Meier B, Imani J, Kogel K-H, Peiter E, Vothknecht UC, Chigri F. 2022. Comparative analysis of stress-induced calcium signals in the crop species barley and the model plant *Arabidopsis thaliana*. BMC Plant Biology **22**, 447.

Gol L, Haraldsson EB, von Korff M. 2021. *Ppd-H1* integrates drought stress signals to control spike development and flowering time in barley. Journal of Experimental Botany **72**, 122–136.

Gutscher M, Pauleau A-L, Marty L, Brach T, Wabnitz GH, Samstag Y, Meyer AJ, Dick TP. 2008. Real-time imaging of the intracellular glutathione redox potential. Nature Methods **5**, 553–559.

Hasan MS, Chopra D, Damm A, Koprivova A, Kopriva S, Meyer AJ, Müller-Schüssele S, Grundler FMW, Siddique S. 2022. Glutathione contributes to plant defence against parasitic cyst nematodes. Molecular Plant Pathology **23**, 1048–1059.

Haugland RP, Spence MTZ, Johnson ID. 1996. Handbook of fluorescent probes and research chemicals. Eugene, OR: Molecular Probes.

Hernanz D, Nuñez V, Sancho AI, Faulds CB, Williamson G, Bartolomé B, Gómez-Cordovés C. 2001. Hydroxycinnamic acids and ferulic acid dehydrodimers in barley and processed barley. Journal of Agricultural and Food Chemistry **49**, 4884–4888.

Himmelbach A, Zierold U, Hensel G, Riechen J, Douchkov D, Schweizer P, Kumlehn J. 2007. A set of modular binary vectors for transformation of cereals. Plant Physiology **145**, 1192–1200.

Hipsch M, Lampl N, Zelinger E, Barda O, Waiger D, Rosenwasser S. 2021. Sensing stress responses in potato with whole-plant redox imaging. Plant Physiology **187**, 618–631.

Hoagland DR, Arnon DI. 1938. The water-culture method for growing plants without soil. College of Agriculture, University of California.

Imani J, Li L, Schäfer P, Kogel K-H. 2011. STARTS—a stable root transformation system for rapid functional analyses of proteins of the monocot model plant barley: stable barley root transformation system. The Plant Journal **67**, 726–735.

Kirschner GK, Stahl Y, Imani J, von Korff M, Simon R. 2018. Fluorescent reporter lines for auxin and cytokinin signalling in barley (*Hordeum vulgare*). PLoS One **13**, e0196086.

Kreszies T, Shellakkutti N, Osthoff A, Yu P, Baldauf JA, Zeisler-Diehl VV, Ranathunge K, Hochholdinger F, Schreiber L. 2019. Osmotic stress enhances suberization of apoplastic barriers in barley seminal roots: analysis of chemical, transcriptomic and physiological responses. New Phytologist **221**, 180–194.

Leisen T, Werner J, Pattar P, *et al*. 2022. Multiple knockout mutants reveal a high redundancy of phytotoxic compounds contributing to necrotrophic pathogenesis of *Botrytis cinerea*. PLoS Pathogens **18**, e1010367.

Marty L, Bausewein D, Müller C, *et al*. 2019. Arabidopsis glutathione reductase 2 is indispensable in plastids, while mitochondrial glutathione is safeguarded by additional reduction and transport systems. New Phytologist **224**, 1569–1584.

Marty L, Siala W, Schwarzländer M, Fricker MD, Wirtz M, Sweetlove LJ, Meyer Y, Meyer AJ, Reichheld J-P, Hell R. 2009. The NADPH-dependent thioredoxin system constitutes a functional backup for cytosolic glutathione reductase in Arabidopsis. Proceedings of the National Academy of Sciences, USA **106**, 9109–9114.

Mascher M, Gundlach H, Himmelbach A, *et al*. 2017. A chromosome conformation capture ordered sequence of the barley genome. Nature **544**, 427–433.

Meyer AJ, Brach T, Marty L, Kreye S, Rouhier N, Jacquot J-P, Hell R. 2007. Redox-sensitive GFP in *Arabidopsis thaliana* is a quantitative biosensor for the redox potential of the cellular glutathione redox buffer. The Plant Journal **52**, 973–986.

Meyer AJ, Dreyer A, Ugalde JM, Feitosa-Araujo E, Dietz K-J, Schwarzländer M. 2021. Shifting paradigms and novel players in Cys-based redox regulation and ROS signaling in plants—and where to go next. Biological Chemistry **402**, 399–423.

Meyer AJ, May MJ, Fricker M. 2001. Quantitative *in vivo* measurement of glutathione in Arabidopsis cells: *in vivo* measurement of glutathione. The Plant Journal **27**, 67–78.

Morgan B, Ezeriņa D, Amoako TNE, Riemer J, Seedorf M, Dick TP. 2013. Multiple glutathione disulfide removal pathways mediate cytosolic redox homeostasis. Nature Chemical Biology **9**, 119–125.

Müller N, Leroch M, Schumacher J, *et al*. 2018. Investigations on VELVET regulatory mutants confirm the role of host tissue acidification and secretion of proteins in the pathogenesis of *Botrytis cinerea*. New Phytologist **219**, 1062–1074.

Müller-Schüssele SJ, Bohle F, Rossi J, Trost P, Meyer AJ, Zaffagnini M. 2021a. Plasticity in plastid redox networks: evolution of glutathione-dependent redox cascades and glutathionylation sites. BMC Plant Biology **21**, 322.

Müller-Schüssele SJ, Schwarzländer M, Meyer AJ. 2021b. Live monitoring of plant redox and energy physiology with genetically encoded biosensors. Plant Physiology **186**, 93–109.

Müller-Schüssele SJ, Wang R, Gütle DD, *et al*. 2020. Chloroplasts require glutathione reductase to balance reactive oxygen species and maintain efficient photosynthesis. The Plant Journal **103**, 1140–1154.

Munns R, James RA, Läuchli A. 2006. Approaches to increasing the salt tolerance of wheat and other cereals. Journal of Experimental Botany **57**, 1025–1043.

Muzammil S, Shrestha A, Dadshani S, Pillen K, Siddique S, Léon J, Naz AA. 2018. An ancestral allele of *pyrroline-5-carboxylate synthase1* promotes proline accumulation and drought adaptation in cultivated barley. Plant Physiology **178**, 771–782.

Newton AC, Flavell AJ, George TS, *et al*. 2011. Crops that feed the world 4. Barley: a resilient crop? Strengths and weaknesses in the context of food security. Food Security **3**, 141–178.

Nietzel T, Elsässer M, Ruberti C, *et al*. 2019. The fluorescent protein sensor roGFP2–Orp1 monitors in vivo H_2O_2 and thiol redox integration and elucidates intracellular H_2O_2 dynamics during elicitor-induced oxidative burst in Arabidopsis. New Phytologist **221**, 1649–1664.

Osthoff A, Donà dalle Rose P, Baldauf JA, Piepho H-P, Hochholdinger F. 2019. Transcriptomic reprogramming of barley seminal roots by combined water deficit and salt stress. BMC Genomics **20**, 325.

Rey P, Tarrago L. 2018. Physiological roles of plant methionine sulfoxide reductases in redox homeostasis and signaling. Antioxidants **7**, 114.

Schwarzländer M, Dick TP, Meyer AJ, Morgan B. 2016. Dissecting redox biology using fluorescent protein sensors. Antioxidants & Redox Signaling **24**, 680–712.

Schwarzländer M, Fricker MD, Müller C, Marty L, Brach T, Novak J, Sweetlove LJ, Hell R, Meyer AJ. 2008. Confocal imaging of glutathione redox potential in living plant cells. Journal of Microscopy **231**, 299–316.

Schwarzländer M, Fricker MD, Sweetlove LJ. 2009. Monitoring the *in vivo* redox state of plant mitochondria: effect of respiratory inhibitors, abiotic stress and assessment of recovery from oxidative challenge. Biochimica et Biophysica Acta **1787**, 468–475.

Smith IK, Vierheller TL, Thorne CA. 1988. Assay of glutathione reductase in crude tissue homogenates using 5,5′-dithiobis(2-nitrobenzoic acid). Analytical Biochemistry **175**, 408–413.

Ugalde JM, Fecker L, Schwarzländer M, Müller-Schüssele SJ, Meyer AJ. 2022. Live monitoring of ROS-induced cytosolic redox changes with roGFP2-based sensors in plants. Methods in Molecular Biology **2526**, 65–85.

Ugalde JM, Fuchs P, Nietzel T, Cutolo EA, Homagk M, Vothknecht UC, Holuigue L, Schwarzländer M, Müller-Schüssele SJ, Meyer AJ. 2021. Chloroplast-derived photo-oxidative stress causes changes in H_2O_2 and E_{GSH} in other subcellular compartments. Plant Physiology **186**, 125–141.

Wagner S, Steinbeck J, Fuchs P, *et al*. 2019. Multiparametric real-time sensing of cytosolic physiology links hypoxia responses to mitochondrial electron transport. New Phytologist **224**, 1668–1684.

Watanabe K, Breier U, Hensel G, Kumlehn J, Schubert I, Reiss B. 2016. Stable gene replacement in barley by targeted double-strand break induction. Journal of Experimental Botany **67**, 1433–1445.